JOURNAL OF COMPUTATIONAL PHYSICS 6, 68–94 (1970)

A Computer Study of Finite-Amplitude Water Waves

ROBERT K.-C. CHAN AND ROBERT L. STREET

Department of Civil Engineering, Stanford University, Stanford, California 94305

Received October 7, 1969

The nonlinear properties of finite-amplitude water waves are modelled by a numerical method based on the Marker and Cell technique. The paper introduces the Stanford University Modified MAC (SUMMAC) code which is shown to be a valid tool for analyzing incompressible flows with a free surface under transient conditions. The method is applied as an example to the run up of a solitary wave on a vertical wall. The results are compared critically with available experimental data.

1. INTRODUCTION

An understanding of wave actions is of vital importance in the design of many coastline and harbor structures. A number of failures in the past stemmed from inadequate design which was the consequence of man's limited knowledge about the great ocean storm waves and tsunamis or seismic sea waves. A review of the literature of coastal engineering [1] indicates that the action of water waves in the shallower regions near the shore or the surf zone is known only in terms of the results of experiments and model tests on specific configurations. In addition, the difficulties of making experimental measurements under transient conditions prevent us from acquiring more than a superficial knowledge of the total wave action.

Because of their finite amplitudes, the mathematical description of large water waves in shallow water is necessarily nonlinear [2]. The importance of nonlinearity excludes the possibility of employing the linearized theory which is based on the assumption of small amplitudes [3]. Despite the fact that an increasing number of nonlinear theories are available, applications to practical problems are seriously restricted by the limiting assumptions inherent in these theories. The most common limitations include admissible boundary geometries, restriction to infinite domain, nonuniform satisfaction of the essential free-surface boundary conditions, etc. It appears that comprehensive theoretical tools are needed to provide adequate descriptions of the steady and unsteady motion of finite-amplitude water waves in the near-shore zone.

In view of the continuing and extremely rapid development of high-speed digital computers, we turned to the development of numerical methods as tools for wave analysis. A purpose of this paper is to demonstrate the validity of one numerical method by applying it to a simple, yet practical, problem whose solution properties are well-known and experimentally documented. The employment of our numerical method in more complex problems is discussed at the close of the presentation.

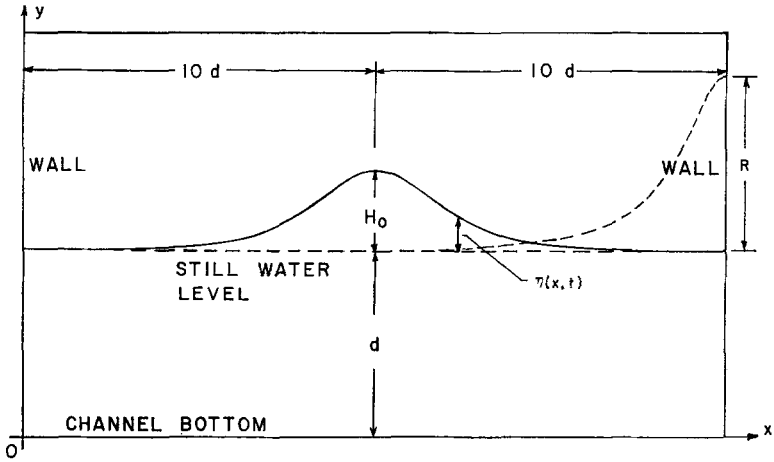

FIG. 1. Definition sketch showing a solitary wave in a channel

This paper deals with the motion of a solitary wave (Fig. 1). A solitary wave is a wave consisting of a single elevation of fluid, of height H_0 not necessarily small compared with the total depth d of the fluid. If properly started, this wave may travel for a considerable distance along a uniform canal, with little or no change of form [3]. Following Jordaan's [4] argument, Camfield and Street [5] suggested that, to study the shoaling, breaking and run-up characteristics of catastrophic ocean waves, it is reasonable to begin by generating and studying simple finite-amplitude waves such as the solitary wave. Because of the availability of a large amount of analytic results and experimental data on this wave, in addition to its practical importance, we have also selected the solitary wave as the medium for the illustration and testing of our numerical method. The objectives of the work were two-fold. First, we wished to show that the numerical technique provides satisfactory predictions of the run-up on a vertical wall. Secondly, we wished to advance the methodology of the Marker and Cell (MAC) numerical technique [6, 7] and develop a valid tool for the analysis of two-dimensional, nonlinear motions.

The computations were performed on an IBM 360/67 system. Graphic outputs of the wave profiles were obtained through the use of a CALCOMP plotter.

2. The Marker and Cell Method

The numerical scheme employed in this work is based on the Marker and Cell (MAC) method originally developed at the Los Alamos Scientific Laboratory, University of California [6, 7]. Welch, et al., [6] gave a detailed description of their original method, flow charts for computations and several examples of numerical solutions.

Basically the method obtains the solution to a set of finite-difference equations that are derived from the partial differential equations and boundary conditions of viscous fluid flow in two space dimensions. The essential physical principles used are the conservation of mass and the momentum theorem (the Navier–Stokes equations). Only nonturbulent flows are considered. Pressure and velocity—the important dependent variables for water waves—are used directly as the primary field variables. A straightforward differencing scheme is used; however, the primary requirement imposed was that both mass conservation and momentum theorem principles be satisfied rigorously in the difference equations as they were in the original differential equations. The method makes use of a rectangular grid of Eulerian calculation cells, in each of which the fluid is characterized by average values of the field variables. The flow boundary conditions are derived from the finite-difference momentum equations and certain symmetry conditions. The initial conditions of a given problem are easily set and operation of the MAC method is then quite simple. Massless "marker" particles are identified along any free surfaces of the problem; these "markers," i.e., the free surface, are advanced in each time step to new positions in accordance with a simple kinematic relation between the surface geometry and fluid velocities.

The original version of the MAC method was used in the early stages of the present investigation. The results were not satisfactory. The computed free-surface profiles were very ragged, indicating considerable errors originating from the treatment of free-surface boundary conditions. Several modifications were made and the result is a quite satisfying procedure. As these changes have a distinct effect on the accuracy of solutions, the changes are described in separate sections.

3. Governing Equations and Auxiliary Conditions

The Navier–Stokes equations are used in the MAC method. When the conservation of mass equation is included and the suitable boundary and initial conditions

are specified, the Navier–Stokes equations are sufficient to determine fluid flow patterns uniquely. Viscous terms are retained in the following derivations and the associated computer program for the sake of generality and so that the program could be used later to study viscous effects and for possible turbulence simulation without major modification. In the present study of water waves, the viscosity was set to zero in the computations. This is consistent with the "free-slip" boundary condition at walls and the free-surface condition described below.

For an incompressible flow the Navier–Stokes equations in two dimensions can be written in the form

$$\frac{\partial u}{\partial t} + \frac{\partial u^2}{\partial x} + \frac{\partial uv}{\partial y} = -\frac{\partial \phi}{\partial x} + g_x + \nu\left(\frac{\partial^2 u}{\partial x^2} + \frac{\partial^2 u}{\partial y^2}\right) \tag{1}$$

$$\frac{\partial v}{\partial t} + \frac{\partial uv}{\partial x} + \frac{\partial v^2}{\partial y} = -\frac{\partial \phi}{\partial y} + g_y + \nu\left(\frac{\partial^2 v}{\partial x^2} + \frac{\partial^2 v}{\partial y^2}\right) \tag{2}$$

and the conservation of mass equation is

$$\frac{\partial u}{\partial x} + \frac{\partial v}{\partial y} = 0. \tag{3}$$

Here, x and y are the coordinates of a fixed Cartesian system; u and v are the velocity components in the x- and y-directions, respectively; ϕ is the ratio of pressure p to the constant density ρ of the fluid (i.e., $\phi \equiv p/\rho$); g_x and g_y are the x and y components of the body acceleration (gravity); and ν is the kinematic viscosity of the fluid. If the field variables u, v, and ϕ are defined at the locations shown in Fig. 2, then it can be shown, by integrating over a fixed control volume,

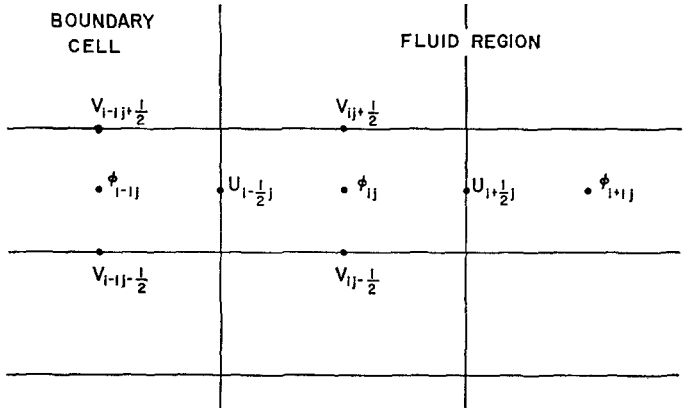

FIG. 2. Position of field variables

that the finite-difference representations of Eqs. (1) and (2) satisfy the momentum principle rigorously [6].

Equations (1) and (2) provide a means of computing $\partial u/\partial t$ and $\partial v/\partial t$ so that the data of u and v can be updated. But this updating procedure requires knowledge of $\partial\phi/\partial x$ and $\partial\phi/\partial y$. Thus, we define

$$D \equiv \frac{\partial u}{\partial x} + \frac{\partial v}{\partial y} \tag{4}$$

and the continuity equation becomes

$$D = 0. \tag{5}$$

Operating with $\partial/\partial x$ on Eq. (1) and with $\partial/\partial y$ on Eq. (2), using $\partial^2/\partial x\,\partial t \equiv \partial^2/\partial t\,\partial x$ and $\partial^2/\partial y\,\partial t \equiv \partial^2/\partial t\,\partial y$, and then adding the resulting equations, we have

$$\frac{\partial^2\phi}{\partial x^2} + \frac{\partial^2\phi}{\partial y^2} = -R \tag{6}$$

where

$$R \equiv \frac{\partial^2 u^2}{\partial x^2} + 2\frac{\partial^2 uv}{\partial x\,\partial y} + \frac{\partial^2 v^2}{\partial y^2} + \frac{\partial D}{\partial t} - \nu\left(\frac{\partial^2 D}{\partial x^2} + \frac{\partial^2 D}{\partial y^2}\right).$$

Equations (1), (2), (5), and (6) constitute the basic equations from which a finite-difference scheme can be readily developed. The need for retention of the D terms in Eq. (6) is reviewed in Section 4.

Two types of boundary conditions are employed in our work. First, let q_N and q_T be the velocity components, normal and tangential, respectively, to a solid wall. For water waves, the effect of viscosity and hence boundary layers is small; accordingly, at the wall we use a "free-slip" boundary condition [6]: $q_N = 0$ and $\partial q_T/\partial N = 0$, which corresponds in fact to the condition for inviscid, irrotational flow at a wall. Second, the free surface as defined here is the interface between a liquid and a massless gas, i.e., between the water in the waves and the (relatively) massless air above the wave. Generally speaking, the stress tangential to the surface must vanish and the stress normal to the surface must exactly balance any externally applied normal stress. However, for incompressible fluids with low viscosity, such as water, it is sufficiently accurate to use only the single condition $\phi = \phi_a$ in lieu of the normal and tangential stress conditions [6]. Under usual circumstances $\phi_a = 0$, but we can also specify $\phi_a = f(x, t)$ along the free surface to generate waves impulsively.

4. Finite-Difference Representations

In order to solve the above partial differential equations by a finite-difference scheme [6], the computation region is divided into a number of rectangular cells

(Fig. 3). Each cell is named or "flagged" as being of a certain type, depending on whether the cell represents a solid wall, a free surface, empty space, a cell full of fluid, and/or a boundary or corner cell. By using these flags, the proper boundary conditions can be applied to the pertinent cells.

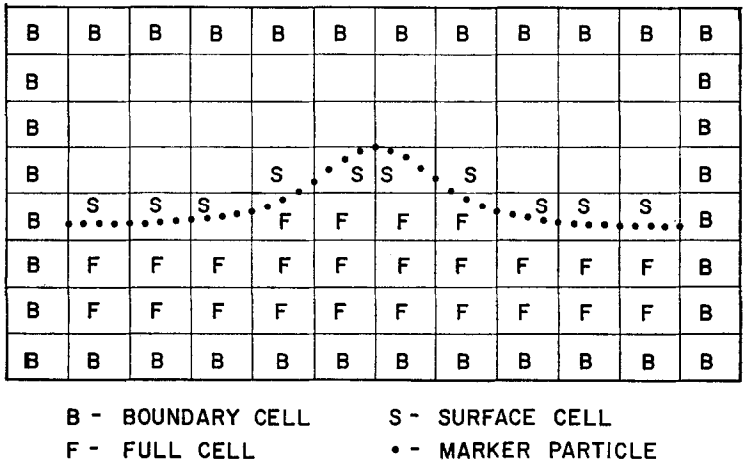

FIG. 3. The Marker-and-Cell setup

In the MAC method $\partial u/\partial t$ is represented by the first-order finite-difference approximation

$$\left(\frac{\partial u}{\partial t}\right)^n \approx \frac{u^{n+1} - u^n}{\delta t} \tag{7}$$

where n refers to the n-th time step and δt is the time increment. This approximation is obviously crude, but the alternatives are not attractive. The permissible size of δt is discussed in Section 11, in connection with the problem of numerical stability. Terms that involve only space derivatives can be approximated more accurately by central differences so from Eqs. (1), (2), (5), and (6), we obtain the finite-difference representations

$$u^{n+1}_{i+1/2j} = u_{i+1/2j} + \delta t \left[\frac{u^2_{ij} - u^2_{i+1j}}{\delta x} + \frac{(uv)_{i+1/2j-1/2} - (uv)_{i+1/2j+1/2}}{\delta y} + g_x + \frac{\phi_{ij} - \phi_{i+1j}}{\delta x} + \nu\left(\frac{u_{i+3/2j} + u_{i-1/2j} - 2u_{i+1/2j}}{\delta x^2} + \frac{u_{i+1/2j+1} + u_{i+1/2j-1} - 2u_{i+1/2j}}{\delta y^2}\right)\right] \tag{8}$$

$$v_{ij+1/2}^{n+1} = v_{ij+1/2} + \delta t \left[\frac{v_{ij}^2 - v_{ij+1}^2}{\delta y} + \frac{(uv)_{i-1/2j+1/2} - (uv)_{i+1/2j+1/2}}{\delta x} + g_v + \frac{\phi_{ij} - \phi_{ij+1}}{\delta y} + \nu \left(\frac{v_{ij+3/2} + v_{ij-1/2} - 2v_{ij+1/2}}{\delta y^2} + \frac{v_{i+1j+1/2} + v_{i-1j+1/2} - 2v_{ij+1/2}}{\delta x^2} \right) \right] \tag{9}$$

$$\phi_{ij} = \frac{1}{Z} \left(\frac{\phi_{i+1j} + \phi_{i-1j}}{\delta x^2} + \frac{\phi_{ij+1} + \phi_{ij-1}}{\delta y^2} + R_{ij} \right). \tag{10}$$

Here

$$Z \equiv 2 \left(\frac{1}{\delta x^2} + \frac{1}{\delta y^2} \right) \tag{11}$$

$$R_{ij} \equiv \frac{(u_{i+1j})^2 + (u_{i-1j})^2 - 2(u_{ij})^2}{\delta x^2} + \frac{(v_{ij+1})^2 + (v_{ij-1})^2 - 2(v_{ij})^2}{\delta y^2} + \frac{2}{\delta x \, \delta y} [(uv)_{i+1/2j+1/2} + (uv)_{i-1/2j-1/2} - (uv)_{i+1/2j-1/2} - (uv)_{i-1/2j+1/2}] - \frac{D_{ij}}{\delta t} - \nu \left(\frac{D_{i+1j} + D_{i-1j} - 2D_{ij}}{\delta x^2} + \frac{D_{ij+1} + D_{ij-1} - 2D_{ij}}{\delta y^2} \right) \tag{12}$$

and

$$D_{ij} \equiv \frac{u_{i+1/2j} - u_{i-1/2j}}{\delta x} + \frac{v_{ij+1/2} - v_{ij+1/2}}{\delta y}. \tag{13}$$

In the above equations, variables with the superscript $n + 1$ are related to the $(n + 1)$-th time step. Variables lacking a superscript are evaluated at the n-th step. Because of the errors introduced in the iterative solution of the pressure field [Eq. (10)], plus the inherent errors in finite differences and roundoff by the computer, the D terms in Eq. (12) do not vanish in general, whereas Eq. (5) indicates that $D \equiv 0$ is required to rigorously conserve mass. Thus, an effort aimed at making $D_{ij} = 0$ at the $(n + 1)$-th step is incorporated into MAC calculations at the n-th time step. Indeed, the precise form of Eq. (10) is obtained by writing Eq. (6) in finite differences and then setting $D_{ij}^{n+1} = 0$. Our derivation of Eqs. (6) and (10) differs in detail from that in MAC [6]; however, the results are precisely the same. The importance of the D terms is discussed in detail by Hirt and Harlow [8].

Only the finite-difference boundary conditions relevant to the solitary wave problem are presented here (cf., [6]). In Fig. 2, cell (i, j) is next to a solid wall and cell $(i - 1, j)$ is a boundary cell. For the "free-slip" boundary we have, from the

difference analogs of the velocity conditions at a wall described above and Eqs. (8) and (13),

(a) $v_{i-1j+1/2} = v_{ij+1/2}$; $\quad v_{i-1j-1/2} = v_{ij-1/2}$

(b) $u^2_{i-1j} = u^2_{ij}$

(c) $(uv)_{i-1/2j+1/2} = 0$; $\quad (uv)_{i-1/2j-1/2} = 0$

(d) $\phi_{i-1j} = \phi_{ij} - g_x \cdot \delta x$

(e) $u_{i-1/2j} = 0$

(f) $D_{i-1j} = D_{ij}$.

Some variables in Eqs. (8)–(12) are not directly defined in the u, v fields. They must be obtained by an interpolation formula. Simple averages are used in the MAC method. For example,

$$\begin{aligned} u_{ij} &= \tfrac{1}{2}(u_{i+1/2j} + u_{i-1/2j}) \\ v_{ij} &= \tfrac{1}{2}(v_{ij+1/2} + v_{ij-1/2}) \\ (uv)_{i+1/2j+1/2} &= \tfrac{1}{2}(u_{i+1/2j} + u_{i+1/2j+1}) \cdot \tfrac{1}{2}(v_{ij+1/2} + v_{i+1j+1/2}). \end{aligned} \tag{14}$$

In the original MAC method $\phi = \phi_a$, the prescribed surface pressure, is assigned to the surface cells. Since the ϕ field is defined at the center of cells, the condition $\phi = \phi_a$ is applied at the *center* of surface cells rather than at the exact location of the free surface. Serious errors may result from this arrangement. It may even create the impression that the MAC method is highly unstable. We shall return to this point in Section 7, where modifications are suggested.

5. Computational Procedures

An initial condition provides the starting values of u and v. Since the initial position of the free surface is known, we can obtain the pressure field by using Eq. (10). But, the value of ϕ at a given cell cannot be calculated directly from this equation because the ϕ values at the neighboring cells are also involved. The field of ϕ values must be obtained simultaneously. The Gauss–Seidel iterative (relaxation) method [9] was used. The ϕ field can be roughly guessed initially–a hydrostatic distribution would be appropriate, for example. Because either ϕ or $\partial\phi/\partial N$, the normal derivative, is specified along the boundaries, convergence of this iterative scheme is guaranteed [9]. Welch, et al., [6] make no recommendations on detailed computational procedures; a method of "over-relaxation" was used here, employing the formula

$$\phi_{\text{new}} = \phi_{\text{old}} + \omega(\phi_{\text{computed}} - \phi_{\text{old}}) \tag{15}$$

where in general the relaxation parameter ω varies from 1.5 to 1.8 for best results.

After solving the pressure field, we use Eqs. (8) and (9) to calculate the new distributions of u and v. At the same time a new free surface geometry is produced by moving the marker particles to their new positions:

$$x_k^{n+1} = x_k^n + u_k \cdot \delta t$$
$$y_k^{n+1} = y_k^n + v_k \cdot \delta t \tag{16}$$

where u_k and v_k denote the velocity components for the k-th particle. The values u_k and v_k are obtained by interpolating from the u and v fields, respectively. For example, if particle k is situated within the zone bounded by the points where u_1, u_2, u_3, and u_4 are defined (Fig. 4), u_k can be computed by

$$u_k = \frac{A_1u_1 + A_2u_2 + A_3u_3 + A_4u_4}{\delta x\, \delta y}. \tag{17}$$

A similar formula is used to calculate v_k.

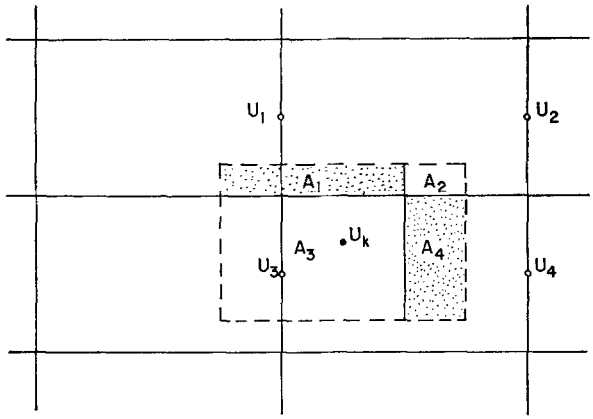

FIG. 4. Linear interpolation for u_k

Now we have completed a cycle of computation, i.e., we have updated the u, v, and ϕ data to a new state. The foregoing procedure is repeated for as many time steps as necessary for the investigation.

6. THE SUMMAC METHOD

Several difficulties arose when we made the first attempt to calculate the motion of large-amplitude water waves by the MAC method. The well-shaped initial

wave became irregular after a few time steps of computation. Also, the u and v fields did not vary as smoothly as they should. Because a small viscosity was used this experience seemed to confirm the statement that the MAC method is numerically unstable for computing low viscosity fluid flows [10].

Usually a formal numerical stability analysis is performed on the governing equations of the problem, such as Eqs. (8) and (9). However, improperly applied boundary conditions may be a more serious source of errors than the governing equations. We have found by experience that the original MAC method can be modified to yield very satisfactory results. Most of the changes have to do with the free-surface condition. This particular condition is inherently difficult to apply in the rectangular mesh system due to the complexity of the surface geometry.

The modifications presented here were developed by heuristic reasoning since a rigorous numerical analysis is difficult, if not impossible. Nevertheless, the modified scheme, called the Stanford University Modified Marker and Cell method (SUMMAC), has been tested and has produced good results.

7. Irregular Stars

It is not proper to impose the condition $\phi = \phi_a$ at the center of surface cells. Only at the free surface, which does not necessarily coincide with surface cell centers, is $\phi = \phi_a$. This difference affects the accuracy of the solution of the ϕ field which in turn influences the calculations of the u and v fields. Unfortunately,

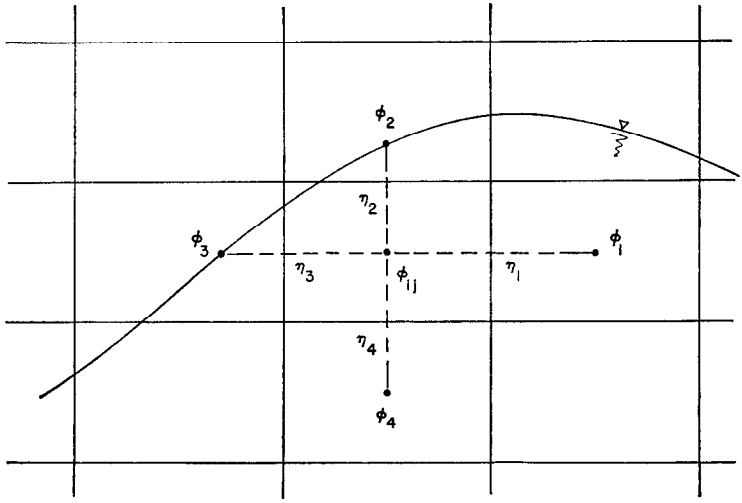

Fig. 5. Irregular star near a curved boundary

features near a curved boundary cannot be adequately resolved by a finite-difference scheme unless "irregular stars" (Fig. 5) are used. Therefore, we derived a finite-difference form of Eq. (6) and used it to apply $\phi = \phi_a$ at the exact location of the free surface by employment of irregular stars.

Let η_1, η_2, η_3, and η_4 be the lengths of the four legs (Fig. 5) and ϕ_1, ϕ_2, ϕ_3, ϕ_4 be the values of ϕ at the ends of the legs. Using the Taylor series expansion [11], we write

$$\phi_1 = \phi_{ij} + \eta_1 \left(\frac{\partial \phi}{\partial x}\right)_{ij} + \frac{\eta_1^2}{2} \left(\frac{\partial^2 \phi}{\partial x^2}\right)_{ij} + 0(\eta_1^3) \tag{18}$$

$$\phi_3 = \phi_{ij} - \eta_3 \left(\frac{\partial \phi}{\partial x}\right)_{ij} + \frac{\eta_3^2}{2} \left(\frac{\partial^2 \phi}{\partial x^2}\right)_{ij} - 0(\eta_3^3) \tag{19}$$

$$\phi_2 = \phi_{ij} + \eta_2 \left(\frac{\partial \phi}{\partial y}\right)_{ij} + \frac{\eta_2^2}{2} \left(\frac{\partial^2 \phi}{\partial y^2}\right)_{ij} + 0(\eta_2^3) \tag{20}$$

$$\phi_4 = \phi_{ij} - \eta_4 \left(\frac{\partial \phi}{\partial y}\right)_{ij} + \frac{\eta_4^2}{2} \left(\frac{\partial^2 \phi}{\partial y^2}\right)_{ij} - 0(\eta_4^3). \tag{21}$$

We neglect terms of the order η_1^3, η_2^3, etc., or higher. Then, by eliminating the $(\partial\phi/\partial x)_{ij}$ term between Eqs. (18) and (19), we obtain

$$\left(\frac{\partial^2 \phi}{\partial x^2}\right)_{ij} = \frac{2}{\eta_1 \eta_3 (\eta_1 + \eta_3)} [\eta_3 \phi_1 + \eta_1 \phi_3 - (\eta_1 + \eta_3)\, \phi_{ij}]. \tag{22}$$

Similarly, eliminating $(\partial\phi/\partial y)_{ij}$ between Eqs. (20) and (21) gives

$$\left(\frac{\partial^2 \phi}{\partial y^2}\right)_{ij} = \frac{2}{\eta_2 \eta_4 (\eta_2 + \eta_4)} [\eta_4 \phi_2 + \eta_2 \phi_4 - (\eta_2 + \eta_4)\, \phi_{ij}]. \tag{23}$$

Equation (6) now becomes

$$\left(\frac{\partial^2 \phi}{\partial x^2}\right)_{ij} + \left(\frac{\partial^2 \phi}{\partial y^2}\right)_{ij} = -R_{ij}\,. \tag{24}$$

Finally we get

$$\phi_{ij} = \frac{\eta_1 \eta_2 \eta_3 \eta_4}{2(\eta_2 \eta_4 + \eta_1 \eta_3)} \left[\frac{\eta_3 \phi_1 + \eta_1 \phi_3}{\eta_1 \eta_3 \left(\frac{\eta_1 + \eta_3}{2}\right)} + \frac{\eta_4 \phi_2 + \eta_2 \phi_4}{\eta_2 \eta_4 \left(\frac{\eta_2 + \eta_4}{2}\right)} + R_{ij}\right] \tag{25}$$

by substituting Eqs. (22) and (23) into Eq. (24).

Equation (25) reduces to Eq. (10) when applied to an interior cell, where $\eta_1 = \eta_3 = \delta x$, $\eta_2 = \eta_4 = \delta y$, $\phi_1 = \phi_{i+1j}$, $\phi_3 = \phi_{i-1j}$, $\phi_2 = \phi_{ij+1}$ and $\phi_4 = \phi_{ij-1}$. Thus, Eq. (25) is a more general formula for solving the ϕ field.

8. Extrapolation of the Velocity Fields

The quantities u and v are not defined outside the fluid region, but they are needed to carry out the computations using Eqs. (8)–(12) near the free surface and to move the marker particles. For the case shown in Fig. 6, u_2 is set equal to u_1 and v_1 is set equal to v_2 in the MAC method. This arrangement makes $D_{ij} = 0$, but this choice of u_2 and v_1 is arbitrary because $D_{ij} \neq 0$, in general, in a surface cell. Indeed, a significant difference between SUMMAC and MAC is that in SUMMAC $D_{ij} = 0$ only in interior cells. Also, consider the case shown

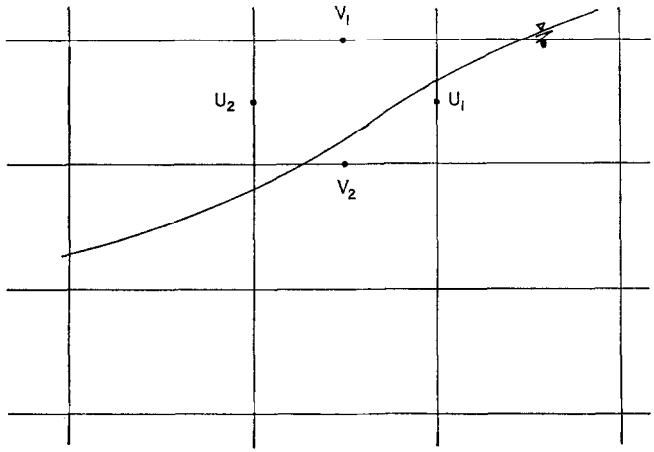

FIG. 6. The undefined variables u_2 and v_1

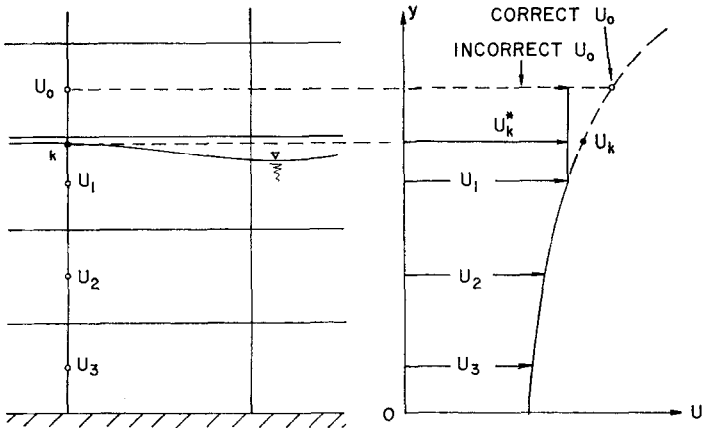

FIG. 7. The Effect of u_0 on u_k

in Fig. 7. Here, u_0 is set equal to u_1 in the unmodified MAC method. Since the particle is to be moved according to the interpolated velocity from the u and v fields, the particle k will assume the erroneous velocity u_k^* instead of the more accurate value u_k.

These problems are resolved by calculating the undefined u and v values through use of a Gregory–Newton backward interpolation formula [12], e.g.,

$$\left(\frac{\partial u}{\partial y}\right)_1 = \frac{1}{\delta y}\left(\tfrac{11}{6}u_1 - 3u_2 + \tfrac{3}{2}u_3 - \tfrac{1}{3}u_4 + \cdots\right). \tag{26}$$

Using $(\partial u/\partial y)_1 \approx (u_0 - u_2)/2\delta y$ in Eq. (26) and rearranging, we have

$$u_0 = \tfrac{11}{3}u_1 - 5u_2 + 3u_3 - \tfrac{2}{3}u_4 . \tag{27}$$

Similar considerations are applied to the extrapolation of v and to other orientations of the free surface. In a given case we extrapolate the u and v fields far enough into the empty space so that all required, but otherwise undefined, variables are established.

9. Calculation of Particle Velocities

The formula used in MAC to obtain particle velocities from the u and v fields is a bivariate linear interpolation formula [see Eq. (17)]. This is adequate in a region where u and v change slowly and monotonically. When the particle is situated near the maxima or minima of the velocity fields (Fig. 8), however, the linearly interpolated particle velocity can be erroneous.

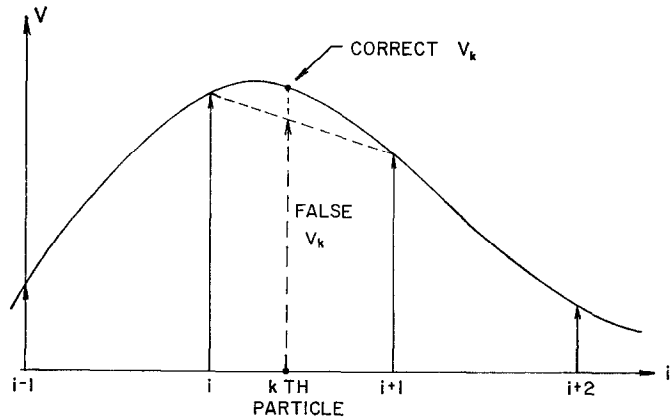

Fig. 8. Interpolation near a maximum

To derive a more satisfactory interpolation formula, consider the particle k in Fig. 9. If the particle lies in the shaded area, we can find the velocity component u_k for the particle by making a Taylor series expansion about the point 0. Neglecting the third and higher order terms, we have

$$u_k = u_0 + h\left(\frac{\partial u}{\partial x}\right)_0 + l\left(\frac{\partial u}{\partial y}\right)_0 + \frac{1}{2!}\left[h^2\left(\frac{\partial^2 u}{\partial x^2}\right)_0 + 2hl\left(\frac{\partial^2 u}{\partial x\,\partial y}\right)_0 + l^2\left(\frac{\partial^2 u}{\partial y^2}\right)_0\right] + \cdots$$

$$\approx u_0 + \left(\frac{h}{\delta x}\right)\left(\frac{u_1 - u_3}{2}\right) + \left(\frac{l}{\delta y}\right)\left(\frac{u_2 - u_4}{2}\right)$$

$$+ \frac{1}{2}\left[\left(\frac{h}{\delta x}\right)^2 (u_1 + u_3 - 2u_0) + \left(\frac{l}{\delta y}\right)^2 (u_2 + u_4 - 2u_0)\right.$$

$$\left. + \frac{1}{2}\left(\frac{h}{\delta x}\right)\left(\frac{l}{\delta y}\right)(u_5 - u_6 + u_7 - u_8)\right]. \tag{28}$$

In a similar manner, a formula can be derived to calculate v_k, the y-component of the particle velocity. Here, the use of first and second space derivatives is consistent with the computation formulas for u and v.

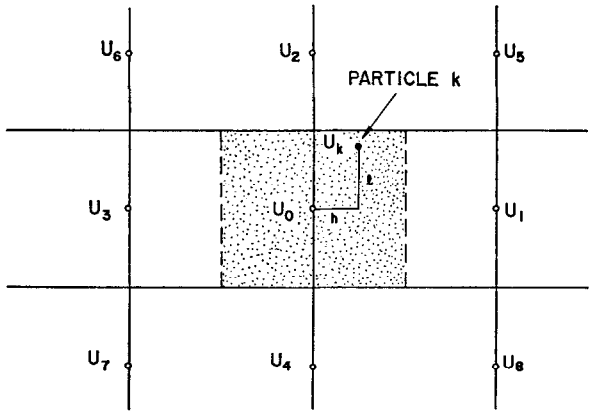

FIG. 9. Second-order interpolation for u_k

10. CALCULATIONS WITH SUMMAC

The flow chart in Fig. 10 gives an outline of the computational procedure of SUMMAC. The general procedure is essentially the same as the one used in the original MAC method [6] and outlined in Sections 2 and 5. However, some

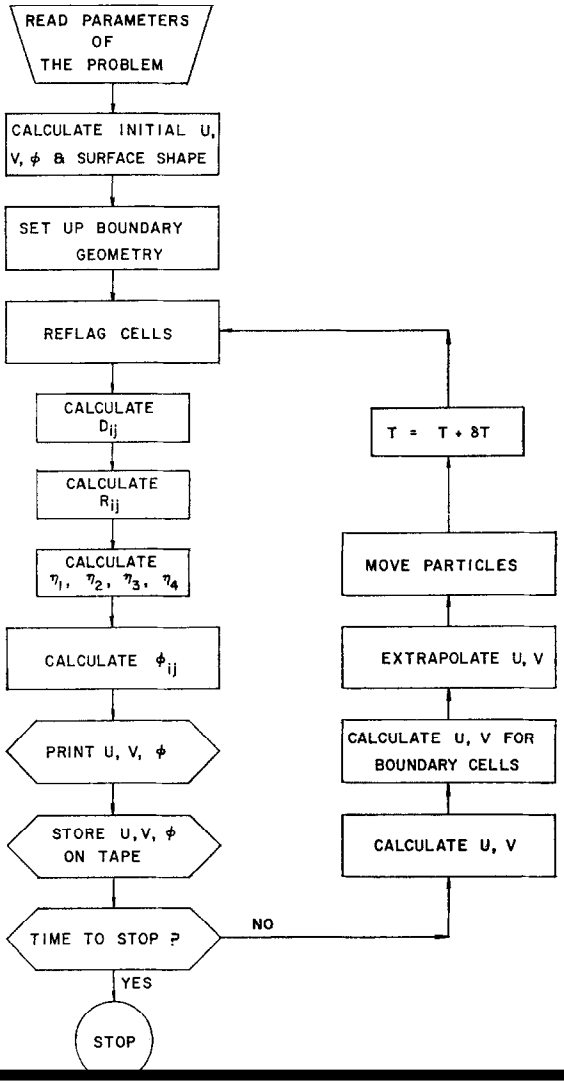

FIG. 10. Flow chart for SUMMAC

additional features are needed to implement the modifications presented in Sections 7–9.

First, a set of input data is used to specify the key parameters of the problem, such as the mesh size, δx, δy, δt, viscosity, etc. Then the cell setup is established by assigning to each cell one or more numerical codes to specify its type. The

initial condition is set by calculating the marker particle positions and the u and v distributions at $t = 0$. Now, we begin the cycle with a procedure that reflags the cells. This procedure has no effect on the first cycle. In the second and future cycles, cells near the free surface must be reflagged from cycle to cycle because of the continuous change of the surface geometry.

To calculate ϕ by Eq. (25), we must know which cells contain an irregular star and the leg lengths η_1, η_2, η_3, η_4. To establish this, we sequentially number (from left to right) the particles that mark the free surface. A cell is then defined to be an "irregular-star cell" if its center lies *on the fluid side* of a free surface which intersects at least one of the four strings connecting the cell center with the centers of the four neighboring cells. If the free surface is represented by many short line segments that connect the surface particles, the distance from the cell center to the free surface gives the length of a leg of the irregular star (Fig. 5). The terms D_{ij} and R_{ij} are needed in computing ϕ_{ij}. As usual we obtain D_{ij} from Eq. (13) and R_{ij} from Eq. (12). Then the values of ϕ are solved simultaneously by the iterative method which was outlined in Section 5, except that Eq. (25) is used for an irregular-star cell and Eq. (10) is used for an interior cell.

Now data of u and v are updated by Eqs. (8) and (9). Remember that these velocity components are evaluated on the borders of cells (Fig. 2). In the SUMMAC method we compute u and v only at locations where they are defined, i.e., within the fluid. For application of Eqs. (8)–(12) near the free surface, the fields of u and v have to be extended to the empty space above the surface. Equation (27) is used for this purpose.

Finally, the marker particles are moved to their new locations by the interpolated velocities obtained from Eq. (28). Then the next time cycle beings with a reflagging of the cells and the process cited above is repeated.

11. Stablility Considerations

The nonlinearity of the Navier–Stokes equations that are used in the MAC or SUMMAC methods makes it difficult to perform rigorous stability analyses. For linear finite-difference equations with constant coefficients, stability can be determined by using a Fourier method proposed by von Neumann [10]. Unfortunately, most equations of physical interest are either nonlinear, have variable coefficients, or both. A powerful and novel method was proposed by Hirt [10] for investigating the computational stability of such nonlinear finite-difference equations.

Hirt reduced a finite-difference equation to a differential equation by expanding each of the difference-function terms in a Taylor series. The lowest order terms in the expansion represent the original differential equation being approximated.

All higher order terms constitute the truncation errors caused by the finite-difference approximation. The stability of a finite-difference equation can often be determined from an examination of these truncation errors [10]. If only diffusion-like truncation errors are retained to order δt and δx^2, the finite-difference equations (8) and (9) can be reduced, respectively, to

$$\frac{\partial u}{\partial t} + \frac{\partial u^2}{\partial x} + \frac{\partial uv}{\partial y} + \frac{\partial \phi}{\partial x} - g_x = \left(\nu - \frac{\delta t}{2} u^2 - \frac{\delta x^2}{2} \frac{\partial u}{\partial x}\right) \frac{\partial^2 u}{\partial x^2} + \left(\nu - \frac{\delta t}{2} v^2 - \frac{\delta y^2}{4} \frac{\partial v}{\partial y}\right) \frac{\partial^2 u}{\partial y^2} \tag{29}$$

$$\frac{\partial v}{\partial t} + \frac{\partial uv}{\partial x} + \frac{\partial v^2}{\partial y} + \frac{\partial \phi}{\partial y} - g_y = \left(\nu - \frac{\delta t}{2} u^2 - \frac{\delta x^2}{4} \frac{\partial u}{\partial x}\right) \frac{\partial^2 v}{\partial x^2} + \left(\nu - \frac{\delta t}{2} v^2 - \frac{\delta y^2}{2} \frac{\partial v}{\partial y}\right) \frac{\partial^2 v}{\partial y^2}. \tag{30}$$

In comparing Eqs. (29) and (30) with Eqs. (1) and (2), we find additional terms in Eqs. (29) and (30). Those terms involving δt result from the first-order approximation to $\partial u/\partial t$ and $\partial v/\partial t$ [see Eq. (7)], while terms containing δx^2 or δy^2 stem from evaluating undefined variables by simple average formulas such as Eqs. (14) and from computing derivatives of u^2, uv, and v^2 terms. These additional terms represent negative diffusion coefficients so that the finite-difference scheme might yield growing unstable solutions if the viscosity ν is smaller than the truncation error terms. Thus, according to Hirt, the stability conditions for the MAC method should be

$$\delta t < \frac{2\nu}{\bar{u}^2} \quad \text{and} \quad \delta x^2 < \frac{2\nu}{\left(\frac{\partial \bar{u}}{\partial x}\right)} \tag{31}$$

where $\bar{u}$ is the average maximum fluid speeds and $\partial \bar{u}/\partial x$ is the average maximum velocity gradient in the direction of flow.

Equations (31) imply that very fine time steps and space increments are required in computing low viscosity fluid motions. In our early attempts to apply the MAC method to the study of water waves we were plagued by the fast development of instabilities which were manifested by very irregular surface profile and field variable distributions. Because small viscosity was used ($\nu/d\sqrt{gd} < 1.8 \times 10^{-6}$), it was suspected that the MAC method would not be suitable for computing flows with very small viscosity. Then, we tested the same problem by using a very large viscosity ($\nu/d\sqrt{gd} = 0.10$), which was more than that required to meet the conditions of Eqs. (31). In the resulting fluid motion the wave speed was found to be incorrect compared to experiment; this may be due to the effect of ν on the

assumed free surface condition $\phi_a = 0$ (see Hirt and Shannon [13]). The instabilities remained, also. We were therefore led to examine the MAC method more carefully. The modifications which have been made were discussed earlier in Sections 7–10. We shall demonstrate the improvement in Section 12 by comparing the parallel results given by the MAC and the SUMMAC methods. A refinement in the evaluation of undefined variables through the use of higher-order interpolations was examined; but as it only reduces the truncation terms involving δx^2 or δy^2 in Eqs. (29) and (30) by a factor of $\frac{1}{2}$ and has no apparent effect on the calculations, the refinement was not pursued. With the SUMMAC method, the only stability conditions that apparently need consideration are these related to the selection of δt. Because viscosity was not used to stabilize or otherwise control computations in our numerical experiment, we presume that δt is restricted only by the Courant stability criterion [6]

$$C\delta t < \frac{2\delta x\, \delta y}{\delta x + \delta y} \tag{32}$$

(where C is the speed of the surface wave) which restricts the distance a wave travels in one time step to less than one space interval. (The diffusional stability condition [6]

$$\nu\delta t < \frac{1}{2}\left(\frac{\delta x^2\, \delta y^2}{\delta x^2 + \delta y^2}\right)$$

presents no restriction at all on zero or very low viscosity calculations.) The application of the Courant condition to nonlinear systems of equations is based on a heuristic extension of linear concepts rather than on direct, rigorous theory.

By using the Courant condition to choose δt, we have obtained very satisfactory results for up to 1000 time steps, provided δx and δy are of such sizes that important features in the fluid motion are sufficiently resolved. It appears that instability problems have been avoided in large part in the SUMMAC method; we believe that the free-surface modifications are the key changes leading to stable computations in this case. A self-correcting mechanism, namely the presence of D terms in Eq. (12), operates in the MAC and SUMMAC methods. This corrective effect, that results from setting $D_{ij}^{n+1} = 0$ in the finite-difference form of Eq. (6) which leads to Eq. (12) and from the interaction between the equations used to find ϕ^n, u^{n+1} and v^{n+1}, suppresses the accumulation of D or incompressibility errors [8] and apparently stabilizes the entire computation. Hirt's stability analysis that led to Eqs. (29) and (30) did not include the effect of D terms. The formidable task of fully analyzing this particular feature of the MAC method remains to be done. One way to test the effect of the D terms in Eq. (12) is a direct numerical experiment on two parallel computer programs, one of which contains the D terms while the other does not. In the present cases, computations without D terms, i.e.,

assuming all $D_{ij} = 0$ in Eq. (12), were unusable because the D_{ij} grew rapidly with increasing time and the computations did not remain well-behaved.

12. Results and Conclusions

As an application of the SUMMAC method, the run up R of a solitary wave on a vertical wall has been calculated for a range of H_0/d (see Fig. 1). Laitone's [14] formulas for the free-surface profile and velocity and pressure fields of a solitary wave moving over a horizontal bottom were used to compute the initial conditions of the incident wave. Laitone used a perturbation method to obtain approximate solutions to models of solitary waves in steady motion. The setup of the computation region is shown in Fig. 1.

Theoretically, the length L of a solitary wave is infinite and Laitone's formulas hold for an infinitely long channel only. Because the computations must be done in a finite domain and the fluid at a distance from the wave crest is essentially still, it is desirable to define a finite, practical length of the solitary wave. The main consideration is that the two vertical walls which constitute the boundaries of the computation region should be far enough from the initial wave crest so that the motion of a solitary wave into the still water in front of a vertical wall can be closely approximated. For this purpose the effective wave length L was obtained by taking $L/2$ equal to the distance from the wave crest to the section where $\eta = 0.01H_0$ according to Laitone's formulas; thus,

$$\frac{L}{d} = 6.90\left(\frac{d}{H_0}\right)^{1/2}. \tag{33}$$

It is seen that the practical length of a solitary wave increases as the amplitude decreases. The two vertical walls have to be located at least $L/2$ away from the initial wave crest. When $H_0/d = 0.1$, for example, the value of $L/2$ as given by Eq. (33) is about 11d. As shown in Fig. 1, the walls were set 10d from the initial wave crest. Since L is even shorter for higher amplitudes, this setup is adequate for $H_0/d > 0.1$. We also set the left-hand wall at 5d behind the initial wave crest. This arrangement resulted in a slight reduction of the run up on the right-hand wall because the moving water in the region beyond the left-hand wall that could have contributed to the run up was eliminated by the left-hand wall. Thus, it is important not to set the walls too close to the initial position of the wave crest.

A mesh of 40 cells in the x-direction and 25 cells in the y-direction was used to represent the computation region. We used $\delta x = 0.5$ and $\delta y = 0.1$ for the case $H_0/d = 0.2$. The reason for using much smaller vertical than horizontal spacing is that we know *a priori* that the field variables change more rapidly in the vertical

direction than in the horizontal direction. As an experiment, a finer mesh, with $\delta x = 0.25$ and $\delta y = 0.08$, was also used to compute the same case. The difference in the results was, however, insignificant. The Courant condition, Eq. (32), was used to determine the time increment δt. The speed of wave C is approximately $(1 + 0.2)^{1/2} = 1.095$ for $H_0/d = 0.2$. Then, from Eq. (32),

$$\delta t < \frac{1}{1.095} \cdot \frac{2(0.5)(0.1)}{0.5 + 0.1} = 0.152 \tag{34}$$

We chose a moderate value of $\delta t = 0.10$ for our computations. We also tried $\delta t = 0.05$ and $\delta t = 0.20$. The use of $\delta t = 0.20$, which violates Eq. (34), resulted in a significantly different solution with a sign of instability in the distributions of the field variables. When $\delta t = 0.05$, we found a small amount of improvement on the solution obtained by using $\delta t = 0.10$. The difference is not significant and we are led to believe that further reduction in δt is not necessary.

The viscosity of water has the nondimensional value $\nu/d\sqrt{gd} = 1.8 \times 10^{-6}$. Zero viscosity was used in all the present cases; however, as noted earlier, viscous terms were retained in the derivation and computer program in the expectation that our future studies would involve viscous effects [see Section 13]. We were able to obtain stable solutions for zero viscosity for all cases run (up to a maximum of 1000 time steps).

The wave run up ratio R/d, as computed by the SUMMAC method, is compared with experimental data [5] in Fig. 11. Clearly, the SUMMAC method yields results that are in excellent agreement with experiment. This is expected of numerical methods in which the governing equations and boundary conditions are more or less uniformly approximated by the finite-difference scheme.

The contour lines of the u, v, and ϕ fields are shown in Figs. 12, 13, and 14, respectively. These plots describe the motion of a solitary wave with $H_0/d = 0.5$ as it approaches the wall at $t/\sqrt{d/g} = 5.4$ and are examples of the information that can be obtained. In the present problem we used three rows of marker particles near the free surface; only the row that marks the free-surface position has real significance in our examples and is shown. However, more particles can be used in the interior of the fluid if details on the particle movement there are desired. Generally, we use as few particles as possible to conserve the storage of the computer. Successive stages of wave deformation are shown in Fig. 15 for the case $H_0/d = 0.5$. The free-surface configurations were obtained by plotting the surface particle coordinates using a CALCOMP plotter.

As discussed in Chan, et al., [15], the velocity distributions given by Laitone [14] are not valid for a solitary wave with fairly large amplitude. Generally speaking, a more accurate knowledge of u and v is needed for waves higher than $H_0/d = 0.4$. For the case $H_0/d = 0.5$, an initial condition based on Laitone's perturbation

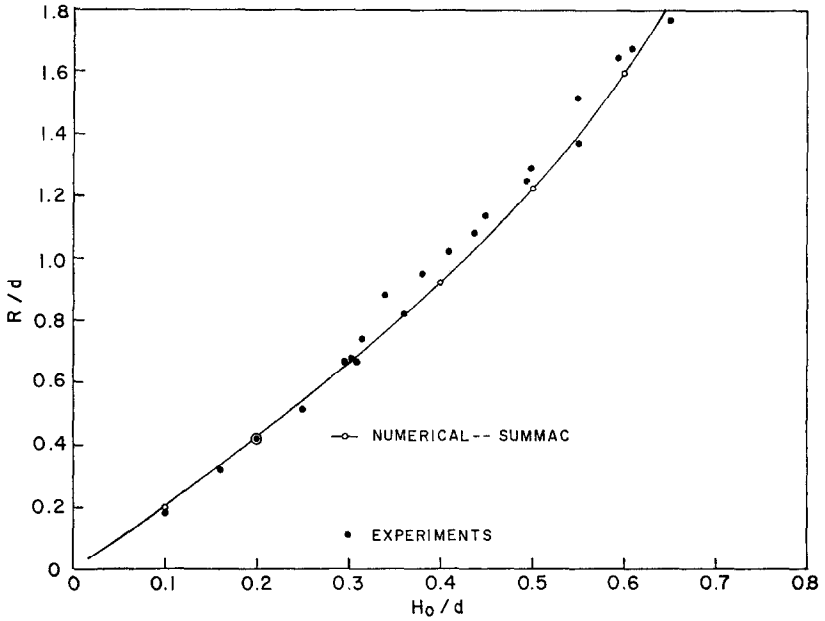

FIG. 11. Wave run up on a vertical wall (R/d)

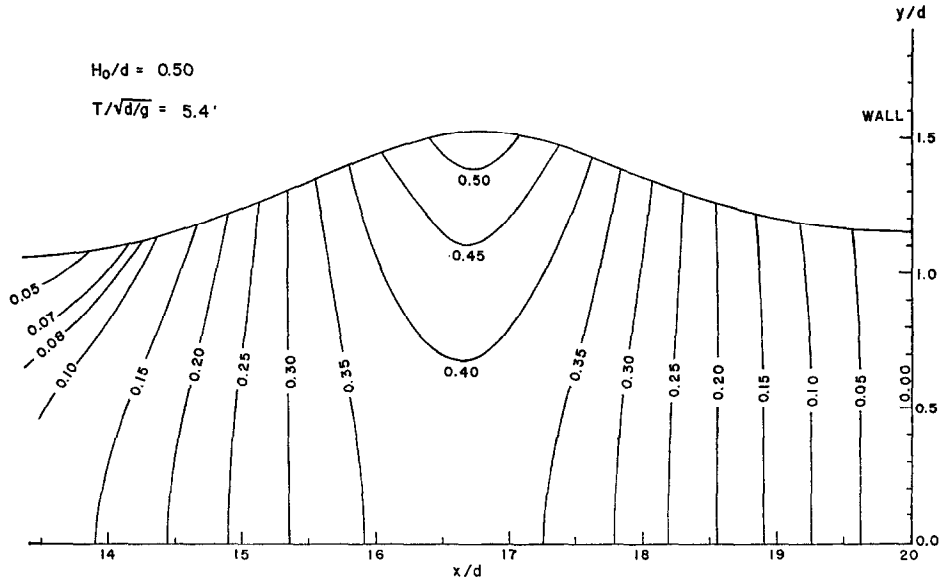

FIG. 12. $u/\sqrt{gd}$ distribution

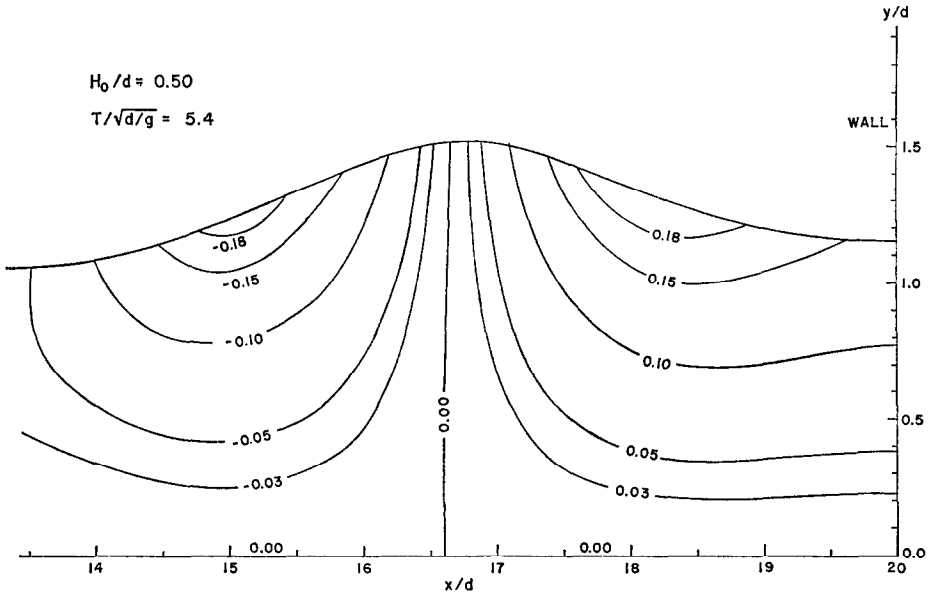

FIG. 13. $v/\sqrt{gd}$ distribution

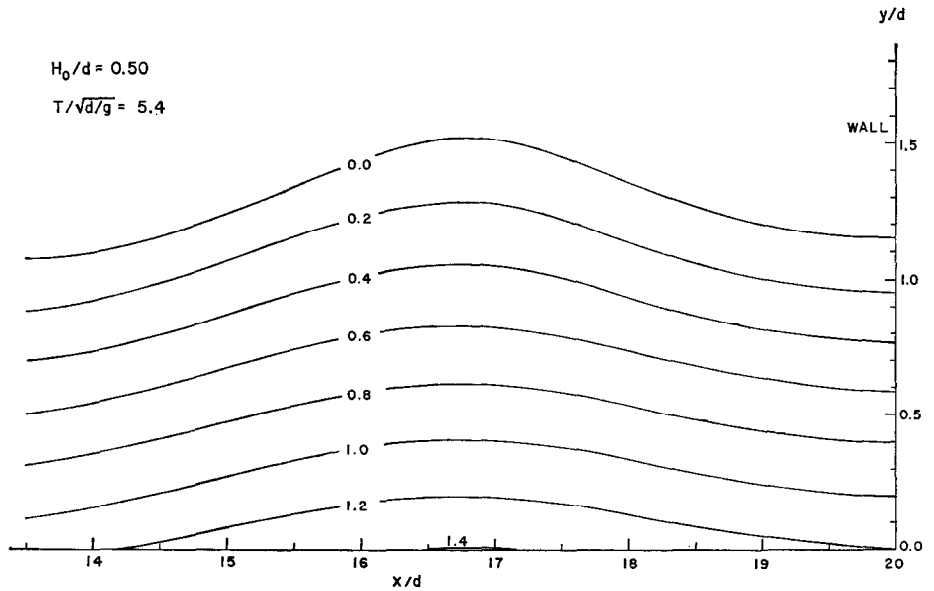

FIG. 14. ϕ distribution

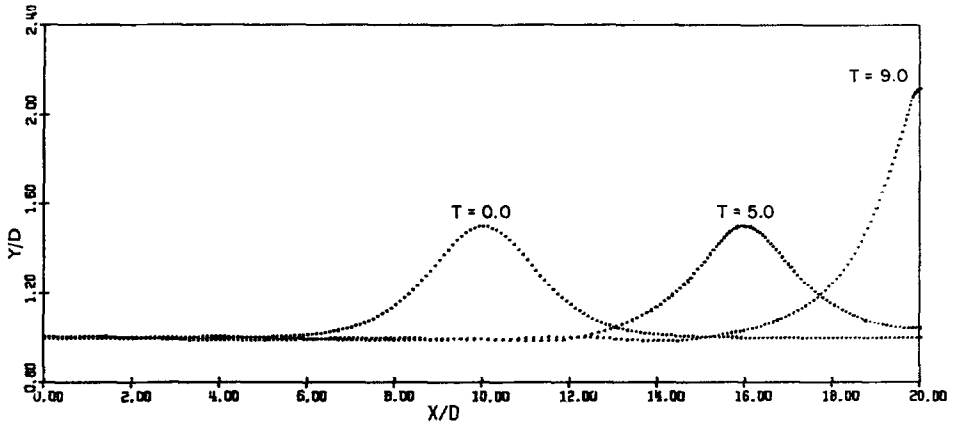

FIG. 15. Wave deformations ($H_0/d = 0.5$)

analysis was tried; however, the condition $D = 0$ was seriously violated in certain parts of the flow region. Also, the resulting wave propagated with an erroneous celerity. To surmount this difficulty, we used a highly accurate steady-state solution which was derived by Chan, et al., [15] as the initial condition for waves with $H_0/d > 0.4$ (in Fig. 15, for example).

In a key test of the method, a wave was reflected from the wall and returned to its initial position for the case $H_0/d = 0.2$. The reflected wave had exactly the same surface profile as its corresponding incident wave. This confirms the observation and expectation that water particles in a totally reflected wave retrace, but in the opposite direction, their original paths in the incident wave.

We have found, by direct numerical tests and comparisons, that the use of irregular stars to compute ϕ_{ij} and the extrapolation of velocity fields had the most drastic effect on the output from the original MAC method. In Fig. 16, the improvement resulting from the more accurate SUMMAC computation of ϕ_{ij} is manifested by the smooth particle alignment on the free surface as contrasted to the highly irregular shape obtained by the unmodified version of the method for waves generated by periodic pressure distribution on the free surface.

To examine the effect of extrapolating the velocity fields near the free surface, we plotted the time history of the horizontal velocity distribution under the wave crest (Fig. 17). On these plots, it is seen that in the original method a decrease in u is incorrectly imposed near the free surface. As time increases, this error is convected with the wave and, at the same time, the error is diffused into the interior of the fluid region. This type of error accounts in part for ragged surface profiles such as that shown in Fig. 16. On the same plots (Fig. 17), velocity profiles of u after the extrapolation and irregular-star modifications were implemented are also shown for comparison.

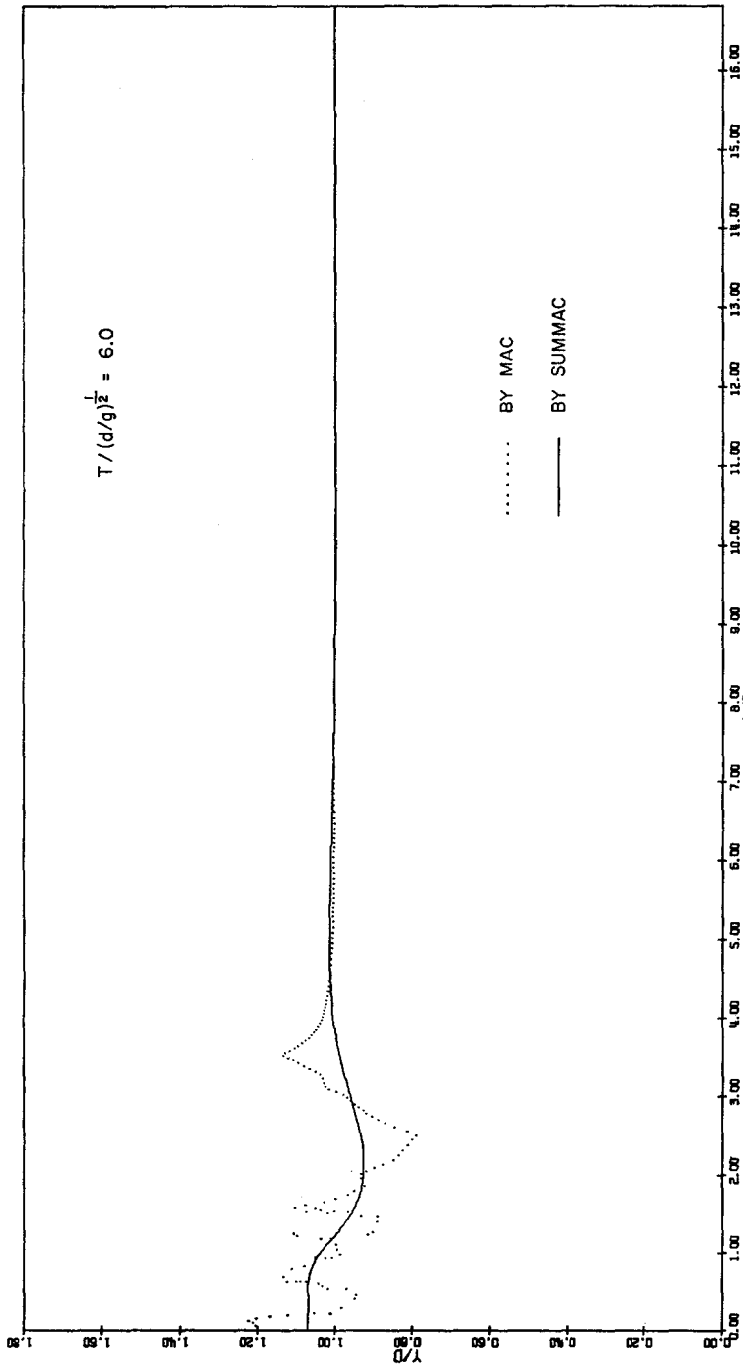

FIG. 16. Comparison of methods

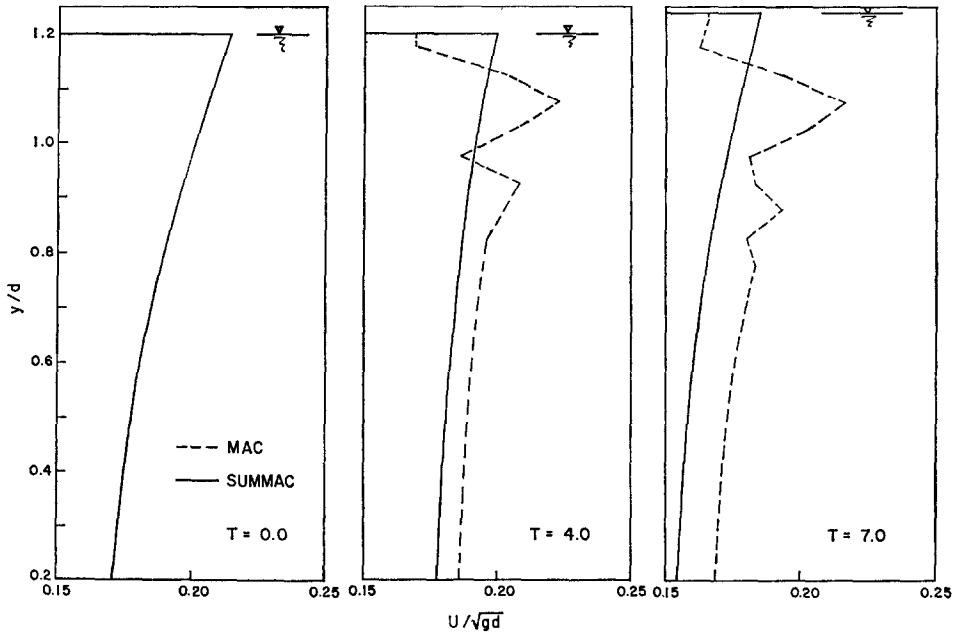

FIG. 17. Comparison of u distribution under the wave crest

The improvement of particle movement through the use of Eq. (28) is prominent only in very curved portions of the free surface, where the linear interpolation formula Eq. (17) tends to level out the curve. In the study of wave run up, for example, the extremely curved water surface near the wall at the maximum run up requires this special treatment.

The application of the SUMMAC method to the present example has been successful. The results presented above clearly indicate that useful and reliable results can be obtained by this numerical method. For the problem under consideration, a typical computation requires about 80 time steps before the maximum run up is reached. This takes about 8 minutes of execution on the IBM 360/67 system. The storage requirement was about 160 K bytes (40,000 words). Thus, the SUMMAC method has been shown to be a feasible method for the study of two-dimensional water waves and their effects on hydraulic structures.